PIV Velocity and Pressure Measurements of the Unsteady Flow Field behind Two Automobile Outside Rear View Mirrors

Bahram Khalighi
Vehicle Development Research Laboratory
General Motors Global R&D
MC 480-106-256
30500 Mound Rd.,
Warren, MI 48090
bahram.khalighi@gm.com

Richard Lee
Research Officer
Aerodynamics Laboratory
NRC Institute for Aerospace Research
1200 Montréal Road
Ottawa, Ontario
Canada K1A 0R6
richard.lee@nrc-cnrc.gc.ca

Abstract: - The unsteady flow fields behind two different automobile outside side rear view mirrors were examined experimentally in order to obtain a comprehensive data base for the validation of the ongoing computational investigation effort to predict the aero-acoustic noise due to the outside rear view mirrors. This study is part of a larger scheme to predict the aero-acoustic noise due to various external components in vehicles. To aid with the characterization of this complex flow field, mean and unsteady surface pressure measurements were undertaken in the wake of two mirror models. Velocity measurements with particle image velocimetry were also conducted to develop the mean velocity field of the wake. Two full-scale mirror models with distinctive geometrical features were investigated.

Key-Words: - PIV measurements, Automobile mirror aerodyanamics, Unsteady flow over outside mirror

1 INTRODUCTION

The unsteady flow field in the wake of the outside rear view mirrors of a typical production car is known to be a significant source of aerodynamic noise. The shape of the mirror assembly, its attitude in relation to the flow and the adjacent windowpane, the details of its installation on the car, and the relative airspeed are all factors that can influence the aero-acoustics performance of cars. Because the wake and adjacent shear layers around a mirror are an important source of noise, a numerical study of the flow field around and in the wake of typical external side-view mirrors was initiated as a collaborative project between General Motors Research and Development Center, and the Center for Turbulence Research at Stanford University. Experimental validation of the predictions is necessary and it is intended to include the characterization of the steady and unsteady pressure in the wake of two mirrors, as well as direct measurements of acoustic radiation in a well-controlled experiment that could be reproduced easily in the computational domain. These validation measurements were organized in a two-phase wind-tunnel test program: The first phase focused on mean and unsteady pressure measurements and mean flow field measurements of the mirror wake; the second phase will concentrate on the measurement of acoustic radiation. This report describes the first phase of the validation program.

2 EXPERIMENTAL DETAILS

The characterization of the unsteady flow field in the wake of the mirrors was performed in the 0.9m Pilot Wind Tunnel at the NRC Institute for Aerospace Research (NRC-IAR) in Canada. Each mirror model was mounted at zero yaw-angle on a ground plane model near the nozzle inlet of the test section (Figure 1). The boundary layer of the oncoming flow field (*i.e.*, velocity and turbulence intensity profiles) and background noise level were characterized as a function of test section velocity at the location of the model without the model in place. An array of static pressure taps and fast-response pressure transducers (microphones) were located on the ground plane in the wake of the mirrors; additional pressure taps were located on the floor upstream of the mirror and on the reflective surface of the mirror. A two-dimensional particle image velocimetry (PIV) system acquired the streamwise (u), lateral (v), and vertical (w) velocity components in the wake region. The mean velocity field was determined for three horizontal planes (the u- and v-components of velocity) and three vertical planes (the u- and w-components).

2.1 The Pilot Wind Tunnel

The Pilot Wind Tunnel at the NRC-IAR is a closed-return facility featuring a ¾-open-jet test section enclosed within a large plenum that is 4 m long, 3 m wide and 2 m high (Figure 1). The cross-sectional dimensions of the nozzle exit are 1 m wide by 0.6 m high, and the highest velocity attainable in the test section is approximately 50 m/s. From a boundary layer survey taken with a two-component hot-film anemometer at the location of the mirror model, the longitudinal and vertical turbulence intensities of the free-stream flow were found to be 0.8% and 1.3%, respectively; the displacement thickness of the boundary layer was estimated to be 4 mm at a velocity of 30 m/s. The experiment was conducted in these smooth flow conditions.

Measurements of the background noise level for an empty test section were acquired with a microphone placed outside the flow of the test section in a quiescent corner of the plenum enclosure. The sound pressure level was found to increase with velocity and reached a level of about 98 dB at a velocity of 30 m/s, the speed at which the majority of testing was performed. No steps were taken in this experiment to insulate the test section against the noise emanating from the fan and the drive motor.

An acoustic resonance or tone in the proximity of 14.5 Hz was known to persist in the plenum. To understand the variation of the tone with wind speed, a survey of unsteady pressure was performed with a differential pressure transducer that sensed fluctuating static pressure on the wall of the nozzle exit. Spectra of root-mean-square pressure (P_{rms}) were developed from the measurements acquired with this pressure transducer. Because the frequency of the tone lay in the vicinity of 14.5 Hz, P_{rms} was formed by integrating a spectral curve over a narrow frequency range of interest, *i.e.*, 13 to 16.5 Hz, and plotted against velocity (Figure 2). The results indicate that P_{rms} increases rapidly after a velocity of 30 m/s, reaching a peak at about 35 m/s. Thus, testing in the vicinity of 35 m/s was avoided to minimize the impact of the acoustic resonance on the measurements of unsteady pressure with the microphones.

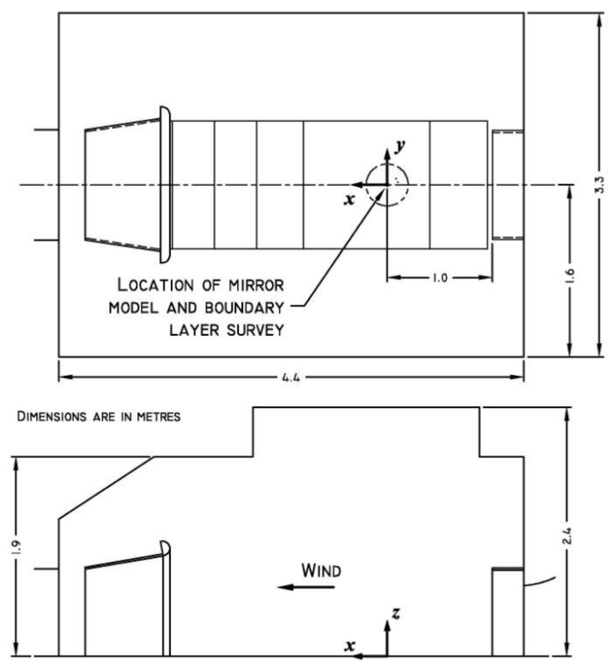

Figure 1. Layout of a mirror model on the ground plane in the 0.9 m Pilot Wind Tunnel and schematic of the plenum.

The coordinate system employed in this paper is defined in Figure 1. The x-axis is aligned with the free-stream flow, the y-axis is normal to the flow in the lateral direction, and the z-axis is normal to the floor of the plenum.

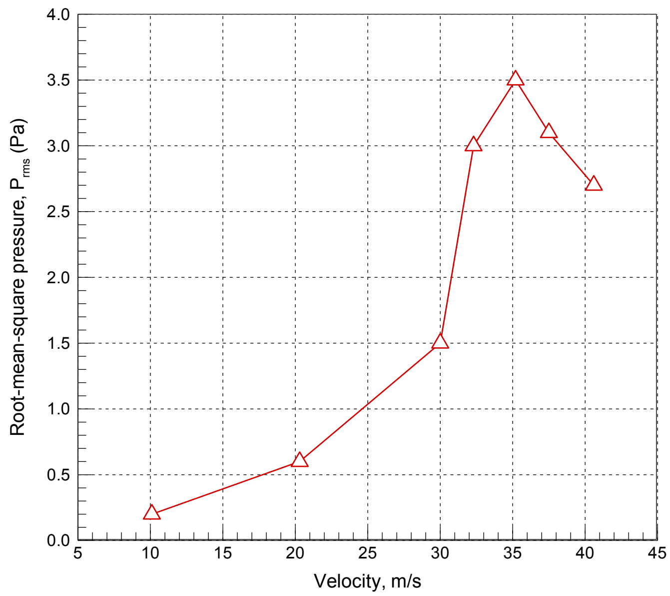

Figure 2. The variation of the level of acoustic resonance in the plenum as a function of velocity without a mirror model in place.

2.2 Mirror Models

Two different full-scale mirror models were used in these tests. The model of the GMT360 mirror, shown in Figure 3a, is generally found on sport-utility vehicles, features distinctly rounded edges on its windward surface, and is the largest of the mirrors. In contrast, the smaller GMX320 mirror, shown in Figure 3b), is typically found on the Cadillac brand and has sharper edges on the windward surface of its body. The models were fabricated from hard plastic and built-up using a stereo-lithographic process. In this paper the components of a mirror are referred to as the main body, the reflective surface, the neck, and the base, as indicated in Figure 3a. Each main body featured a cavity that was covered by a simple imperforated aluminum sheet that served as a representation of the reflective surface. For PIV measurements, the entire surface of each mirror model, including the reflective surface, was painted flat black to mitigate undesirable reflections of laser light. For pressure measurements, the reflective surface was replaced by a thick plastic plate perforated with an array static pressure taps, of which only a few were actually used. To formulate Reynolds number and Strouhal number, the width of the main body at its mid-height was selected as the characteristic length of the mirror. These lengths are 140 mm and 123 mm for GMT360 and GMX320, respectively.

The mirrors were mounted on a flat ground plane model (*e.g.*, the floor of the plenum), which represented the adjacent door window of an automobile. Although the flow in the vicinity of the A-pillar – where side-view mirrors are typically mounted – has an impact on the flow field surrounding the mirror, a flat ground plane was chosen instead to simplify the computational model. Each mirror model was located at the origin of the *x*-*y* coordinate system on the ground plane, as shown in Figure 1. The location of this origin – being 1 m from the nozzle exit – was selected because it falls within a certain range of longitudinal positions for which a blockage correction of the dynamic pressure was not necessary. A zero-yaw orientation was achieved by ensuring that the yaw-reference edge of each model ran parallel with the *x*-axis.

2.2 Mean Pressure Measurements

Measurements from twenty static pressure taps were acquired. Ffifteen static pressure taps were laid on the ground plane along the centerline of the test section – three taps were located upstream of the mirror model and twelve taps were placed in the wake (figure 4). The furthest tap in the wake was located 880 mm from the mirror. Two additional static pressure taps were placed in the wake off the centerline and a further three were installed on the reflective surface of the mirror (figure 5).

Static pressures were measured with two Scanivalve ZOC 23B electronic scanning pressure modules, which have a differential pressure range of 2.5 kPa (10 inches of water) and an accuracy of 5 Pa. The reference pressure for the ZOC modules was taken from inside the plenum, in an area of stagnant flow. Mean pressures were derived from static pressure data acquired at a rate of 100 samples/second for a period of 10 seconds.

2.3 Unsteady Pressure Measurements

Measurements of unsteady pressure with sensitive microphones in the wake of a bluff body have been successfully demonstrated, for example, in the case of a two-dimensional backward-step [1]. In the investigation at the NRC-IAR, Brüel & Kjær Delta Tron pressure-field ¼-inch pre-polarized microphones (Type 4944A) were employed to measure the unsteady surface pressures in the wake of the mirror models. The microphones are vented

for pressure equalization, have a flat pressure-field response from 4 Hz to 70 kHz, and a dynamic range of 30 to 170 dB(A). With protective nose cones removed, thirty-one microphones were flush-mounted in the ground plane with modified Swagelock fittings (Figure 3). The microphones were distributed on the ground plane along the streamwise centerline and along the arcs of three sectors (Figure 4). The furthest arc was 800 mm from the mirror. Of the microphones mounted along the streamwise centerline, some were co-located with static pressure taps with an offset of 12.7 mm between centers. An additional microphone was installed in the reflective surface. Because of the depth of its cavity, two locations on the reflective surface of the GMT360 mirror were possible (Figure 5a); however, only one location was possible on the GMX320 mirror due to its shallower cavity (Figure 5b). Unsteady pressure data was sampled at a rate of 44 kHz for a period of 70 seconds, yielding a frequency bandwidth of at least 20 kHz.

Static pressures were measured with two Scanivalve ZOC 23B electronic scanning pressure modules, which have a differential pressure range of 2.5 kPa (10 inches of water) and an accuracy of 5 Pa. The reference pressure for the ZOC modules was taken from inside the plenum, in an area of stagnant flow. Mean pressures were derived from static pressure data acquired at a rate of 100 samples/second for a period of 10 seconds.

2.3 Unsteady Pressure Measurements

Measurements of unsteady pressure with sensitive microphones in the wake of a bluff body have been successfully demonstrated, for example, in the case of a two-dimensional backward-step [1]. In the investigation at the NRC-IAR, Brüel & Kjær Delta Tron pressure-field ¼-inch pre-polarized microphones (Type 4944A) were employed to measure the unsteady surface pressures in the wake of the mirror models. The microphones are vented for pressure equalization, have a flat pressure-field response from 4 Hz to 70 kHz, and a dynamic range of 30 to 170 dB(A). With protective nose cones removed, thirty-one microphones were flush-mounted in the ground plane with modified Swagelock fittings (Figure 3). The microphones were distributed on the ground plane along the streamwise centerline and along the arcs of three sectors (Figure 4). The furthest arc was 800 mm from the mirror. Of the microphones mounted along the streamwise centerline, some were co-located with static pressure taps with an offset of 12.7 mm between centers. An additional microphone was installed in the reflective surface. Because of the depth of its cavity, two locations on the reflective surface of the GMT360 mirror were possible (Figure 5a); however, only one location was possible on the GMX320 mirror due to its shallower cavity (Figure 5b). Unsteady pressure data was sampled at a rate of 44 kHz for a period of 70 seconds, yielding a frequency bandwidth of at least 20 kHz.

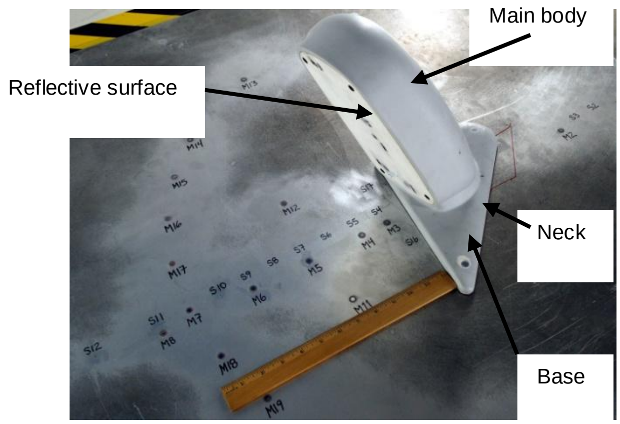

(a) GMT360 mirror model

(b) GMX320 mirror model

Figure 3. Arrangement of the static pressure taps (S) and unsteady pressure transducers, or microphones (M), in the wake of the mirror models.

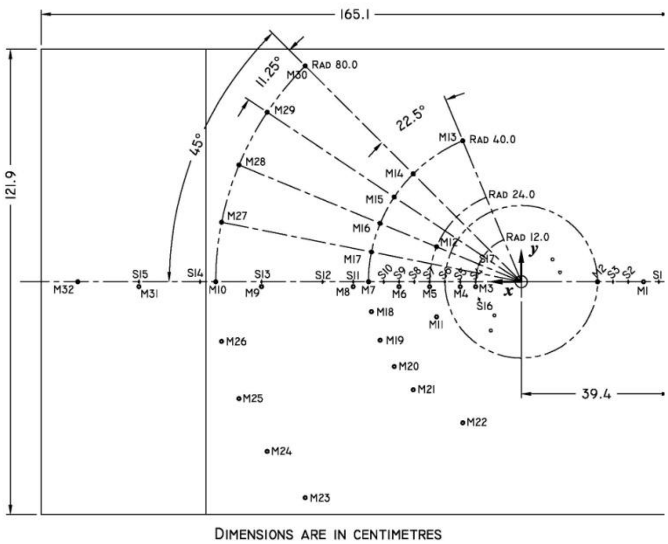

Figure 4. Layout of the static pressure taps and unsteady pressure transducers on the ground plane. The mirror model was centered on the origin of the *x*-*y* axis. **S** Static pressure tap (17 taps), **M** Unsteady pressure transducer (31 microphones)

2.4 Particle Image Velocimetry

Three measurement planes were selected for each view. Two overlapping image segments of the measurement plane covered the near-wake and the far-wake – a distance of approximately 550 mm in the streamwise direction – were adequate to resolve most of the recirculation zone, the freestream, and the shear layer in between. The elevation of the views was concentrated on the wake of the main body of the mirror; the wake of the neck was not surveyed. Two hundred double-frame images (the limit that could be stored in the random access memory of the PIV computer) were typically acquired for each segment of the wake. Details of the PIV recording parameters are listed in Table 1. The INSIGHT™ program, developed by TSI, was used to acquire and analyze the PIV image data. The *deformation grid* scheme – a particle-displacement analysis algorithm appropriate for resolving the details of high shear flows – was employed to compute the particle displacements in the images. Although it was general practice to acquire the maximum number of images possible, not all were required by the particle-displacement analysis algorithm to render a satisfactory mean flow field. The number of images processed varied. In the first segment of the measurement plane that covered the near-wake, only seventy-five were found to be necessary to yield a satisfactory mean flow field. The time to process a set of images in this segment did not exceed two hours (the deformation grid scheme requires about 80 seconds to analyze one pair of full frames). Farther downstream in the second segment, where high shear flow features were less predominant, twenty-five images were processed instead. Within the total observed flow field, approximately 8,500 velocity vectors were resolved at a nominal spatial resolution of 3.5 mm.

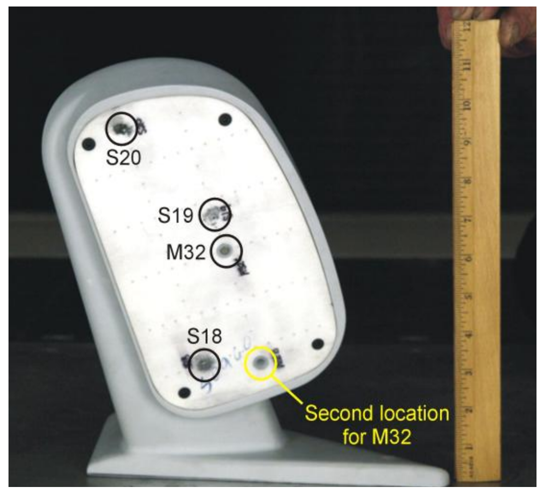

(a) GMT360 mirror model

(b) GMX320 mirror model

Figure 5: Layout of three static pressure taps and one unsteady pressure transducer on the reflective surface of each mirror model.

2.5 Test Program

Both mean and unsteady pressure measurements and PIV measurements were acquired at a common wind speed of 30 m/s. Additional mean pressure and unsteady pressure measurements were acquired 14, 22, and 39 m/s. The mean pressure measurements were acquired first, followed by the unsteady pressure measurements, and then the PIV measurements.

3 RESULTS AND DISCUSSION

3.1 Mean Pressure

The variation of static pressure coefficient (C_P) on the centerline of the ground plane against streamwise distance is plotted in Figure 6 for both mirror models and the baseline case (*i.e.*, with no model in place) over four wind speeds. The results reflect the typical streamwise mean pressure distribution fore and aft of a bluff body. Upstream of the models, the increase of positive C_P, reflects increasing stagnant flow due to the presence of the mirror. Downstream of the models, the results show two distinct features of the flow field, namely a wake and the attachment of the local flow. The presence of significant negative C_P downstream of the leeward face of each mirror reflects the wake of the model. At the streamwise distance where $C_P = 0$, the flow attaches to the ground plane and the recirculation region closes. By this indication, the wake of the GMT360 mirror is slightly longer than that of the GMX320, although the latter generally has a higher negative peak in C_P. The fact that GMT360 is taller by 24 mm may partly account for its longer wake. The results for the wake of GMX320 collapse very well over the four wind speeds; for GMT360, however, the variations in C_P suggest a Reynolds number dependence, which may be attributed to the rounded features of its windward surface. Over the reflective surface of GMT360 the base pressure is reasonably constant, whereas for the GMX320 the base pressure varies significantly over the face.

3.2 Unsteady Pressure

Figures 7 and 8 present typical examples of mean-square spectral distributions and coherence functions for both mirror models at a wind speed of 30 m/s. The spectra were derived from data acquired with the microphones embedded in the ground plane and were computed from an average of ninety-four 32,768-point fast-Fourier transforms (*i.e.*, the entire record was used) of the unbiased time-histories of pressure. All plots of spectra and coherence have a frequency resolution of 1.3 Hz. For the coherence plots, correlations were developed with respect to the farthest downstream microphone, *e.g.*, microphone M31 from the line of microphones that parallels the streamwise centerline (Figure 4).

Flow geometry	**V_∞ = 30 m/s parallel to light sheet**
Maximum in-plane velocity	**$V_\infty \approx$ 35 m/s**
Field of view	**355 mm × 267 mm (W × H)**
Interrogation volume	**7 mm × 7 mm × 1.5 mm (W × H × D)**
Observation distance	***x-y* plane: 859 mm *x-z* plane: 804 mm (GMT360) 940 mm (GMX320)**
Recording method	**15 Hz double frame/single exposure**
Recording medium	**2-megapixel, full frame CCD (1600 × 1200 pixels)**
Recording lens	***f* = 28 mm, f-stop = 1.4**
Illumination	**Nd:YAG laser, 120 mJ/pulse**
Illumination optics	**Light-sheet lens, 20° divergence**
Pulse delay	***x-y* plane: Δt = 12.5 μs *x-z* plane: Δt = 17.5 μs**
Seeding material	**olive oil, d_p = 1.06 μm [2]**

Table 1: PIV recording parameters for mirror wake measurements.

The mean-square spectral distributions and coherence functions for the GMT360 mirror model are shown in Figure 7. In Figure 7a the results presented are for microphones that are located on the streamwise centerline of the ground plane with the exception of microphone M32, which was located on the reflective surface of the mirror shown in Figure 5a. In Figure 7b the microphones are located off the centerline. In both sets of results, the mean-square spectral distributions are dominated by relatively low-frequency turbulent excitation and sharp peaks are clearly evident in the spectra at a frequency of 45.6 Hz (with the exception of microphones M1 and M3). These features are also reflected in the spectra of the corresponding microphones on the opposite side of the centerline. The corresponding Strouhal number (St) is 0.212, based on the characteristic length of the mirror. The results suggest the presence of an alternating trailing vortex system.

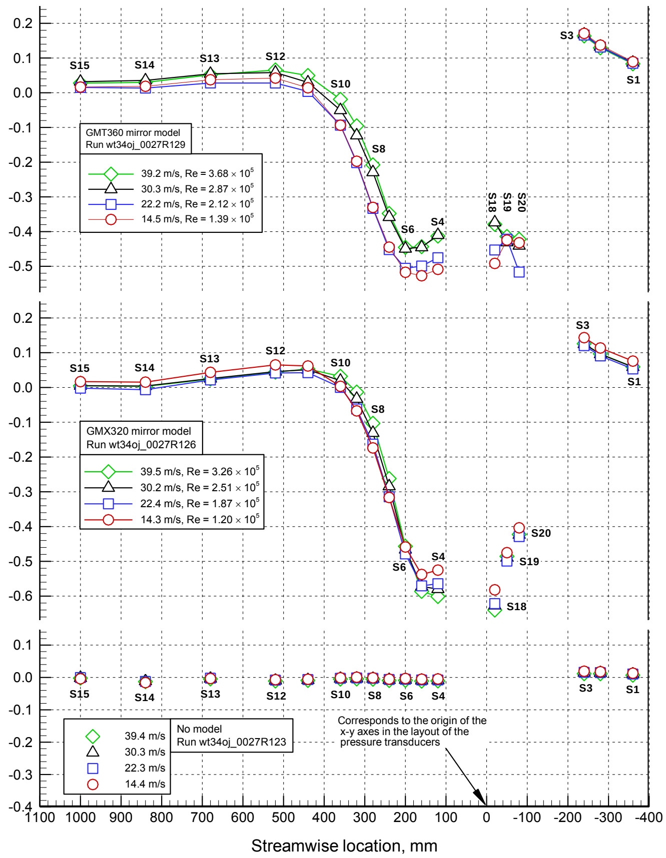

Figure 6. Mean-pressure coefficient on the surface of the ground plane plotted against streamwise-centerline location for both mirror models and the baseline case. The results for the three mean pressure taps placed on the reflective surface (i.e., S18, S19, and S20) are included for the mirror models. The locations of these three pressure taps are not representative.

The case for trailing vortices is substantiated in Figure 7c, which shows that a good correlation exists between the centerline microphone M31 and M10/M9/M8/M6 at a frequency of 45.6 Hz, whereas the correlation between M31 and M1 (located upstream of the model) at the same frequency is weak. The fact that centerline microphones in the wake of the mirror are registering the alternating trailing vortices serves as an indication of the size of these flow structures, which emanate from the sides of the mirror. On another note, a reasonable coherence is observed between M31 and M10/M9/M1 at 13.4 Hz, suggesting that these

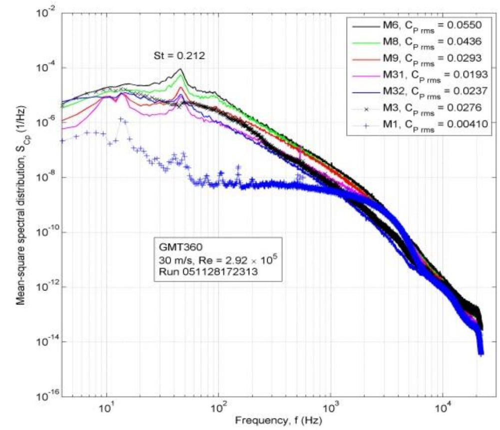

(a) Mean-square spectral distributions for streamwise centerline microphones

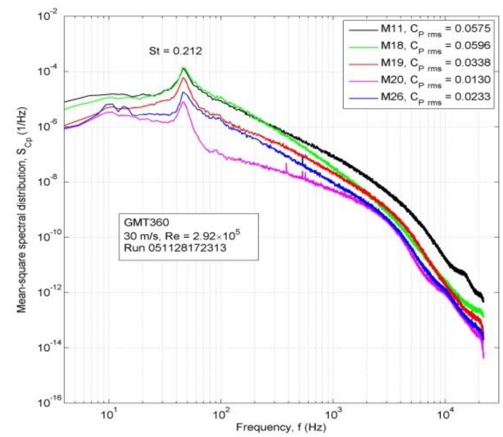

(b) Mean-square spectral distributions for off-centerline microphones

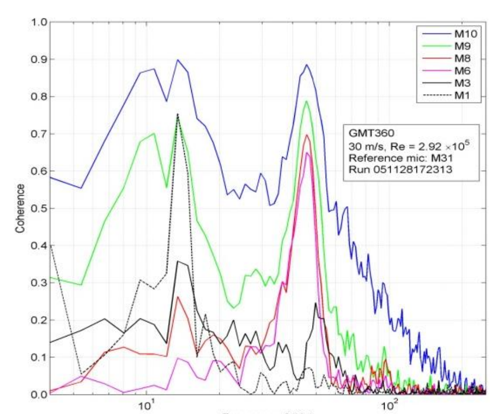

(c) Coherence functions for centerline microphones

Figure 7. Mean-square spectral distributions of pressure coefficient and coherence functions for mirror model GMT360.

microphones registered the acoustic resonance in the plenum. In contrast, the coherences between M31and M8/M6/M3 at 13.4 Hz are relatively weak, an indication perhaps that M8/M6/M3 either lie inside or are in close proximity to the recirculation zone of the wake. If so, then the energy of the turbulent excitation within the recirculation zone dominates the energy of the acoustic resonance.

The mean-square spectral distributions and coherence functions for the GMX320 mirror model are illustrated in Figure 8. The spectra shown in this figure are for the same microphones appearing in Figure 7. In Figure 8a the 45-Hz peak identified previously in the GMT360 results, is conspicuously absent in the spectra for the centerline microphones in the wake of GMX320. However, the spectra for the off-centerline microphones, appearing in Fig. 9b), reveal broad shallow peaks in the proximity of 45 Hz. Again, there exists a degree of symmetry in the spectra for corresponding microphones on both sides of the centerline. It is suggested that these results may be the signature of an *Arch*-type trailing vortex, which sheds as one feature from the GMX320 unlike alternating trailing vortices [3]. If in fact a trailing vortex sheds from GMX320, then the reasonable correlation between M26 and M19/M20 in Figure 8c could be an indicator of its track.

3.3 Mean Velocity Field

Typical contour plots of the mean velocity field captured by the PIV measurements in the *x*-*z* and *x*-*y* planes are shown in Figures 9 and 10 for the GMT360, and in Figures 11 and 12 for the GMX320 mirrors. The velocity contour plots are compositions of two overlapping segments that captured an adequate length of the main-body wake in the measurement plane.

It should be noted that the contour plots are not blended at the juncture of the overlapping segments, nor have the data sets of the segments been integrated. Instead, a composite was formed by overlaying the segments after transforming the local coordinate system of each segment to a common system for the measurement plane (the x_2-y_2 and x_2-z_2 coordinate systems) with its origin located on the reflective surface of the mirror. Each contour plot is accompanied by a series of velocity profiles (*i.e.*, of V_{xz} and V_{xy}) that exemplify the streamwise development of the velocity profile within the wake of the main body. The profiles were extracted from the mean velocity field at intervals of equal distance.

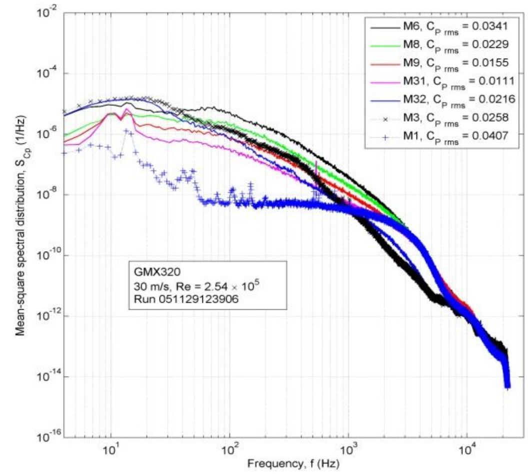

(a) Mean-square spectral distributions for streamwise centerline microphones

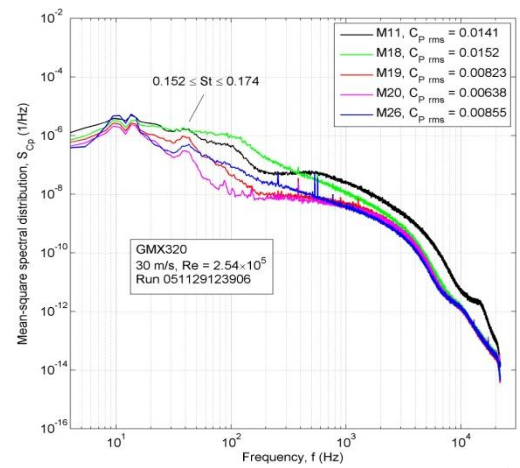

(b) Mean-square spectral distributions for off-centerline microphones

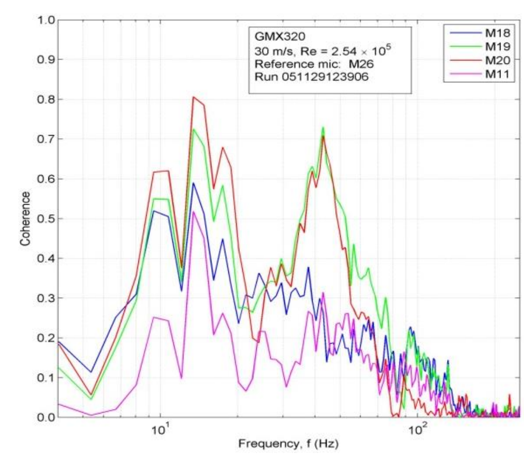

(c) Coherence functions for off-centerline icrophones

Figure 8. Mean-square spectral distributions of pressure coefficient and coherence functions for mirror model GMX320.

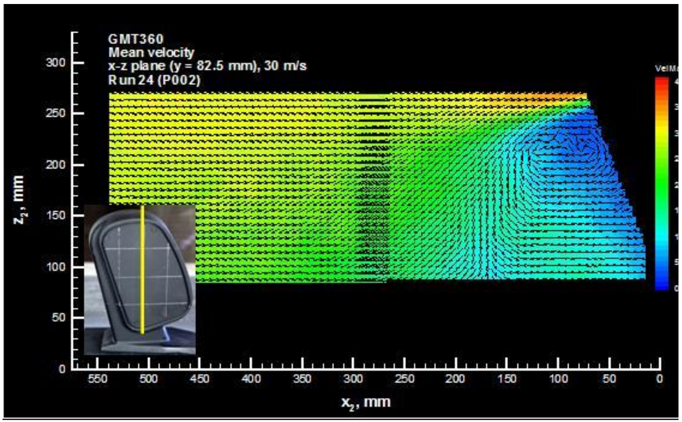

(a) Mean velocity field

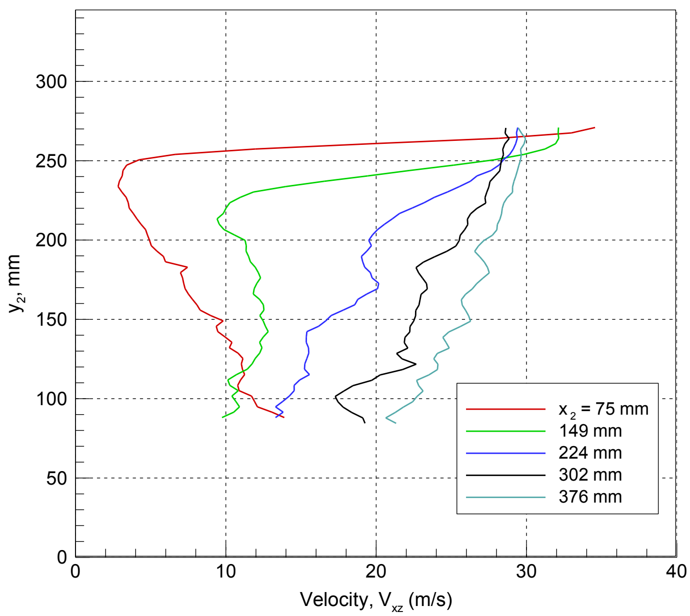

(b) Velocity profiles

Figure 9. Mean velocity field and velocity profiles in the wake (*x-z* plane) of the GMT360 mirror model. In 10a), the magnitude of mean velocity is represented by colored contours and the arrows indicate local flow direction; the inset identifies the measurement plane.

In Figure 9a a number of key features of the mean flow field can be seen in the *x-z* plane of the GMT360. These features are the region of local flow acceleration on the top of the mirror, the high-gradient shear layer that emanates from the top of the mirror, and the recirculation zone over the reflective surface of the mirror. Of particular note is the strong tendency for the shear layer and the freestream to be deflected towards the ground plane. In Figure 9b the velocity profile closest to the reflective surface (x_2 = 75 mm) depicts a large velocity deficit and also a high-gradient shear layer at the top of the mirror. By x_2 = 224 mm the shear layer has diminished and the profiles farther downstream reflect a significant degree of recovery of the velocity deficit.

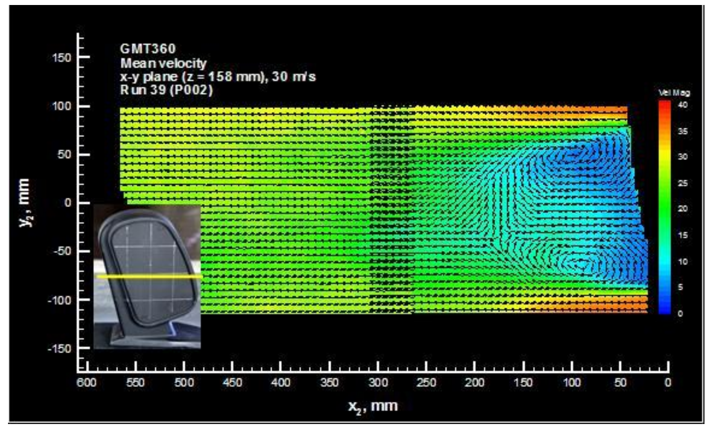

(a) Mean velocity field

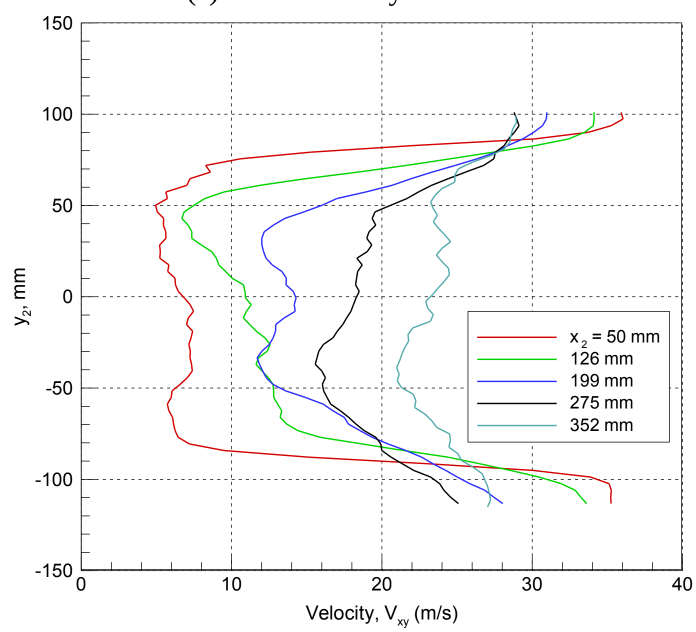

(b) Velocity profiles

Figure 10. Mean velocity field and velocity profiles in the wake (*x-y* plane) of the GMT360 mirror model.

In Figure 10a the recirculation zone, as viewed in the *x-y* plane, features two distinct regions of near-stagnant velocity across the face of the reflective surface. Corresponding with these areas are asymmetrical time-averaged vortex structures that alludes to the presence of an alternating trailing vortex. The sequence of velocity profiles in Figure 10b reveals a velocity recovery comparable to that seen in the *x-z* plane.

The PIV results for GMX320 reveal a different wake structure. In the *x-z* plane, Figure 11a, the shear layer at the top of the mirror is not deflected downward and appears, instead, to remain inline with the freestream flow. In addition, a vortex structure appears near the bottom of the reflective surface, and, at the bottom of the view, there is a significant degree of upward flow, which seems to originate from the region of the neck and the base. In the *x-y* plane in Figure 12a, the hint of a vortex structure on the border of the recirculation zone is insufficient evidence to confirm the presence of *Arch*-type vortices trailing the GMX320, as suggested earlier.

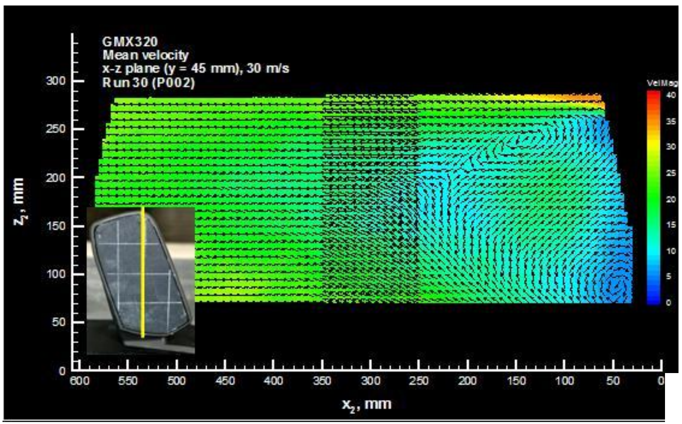

(a) Mean velocity field

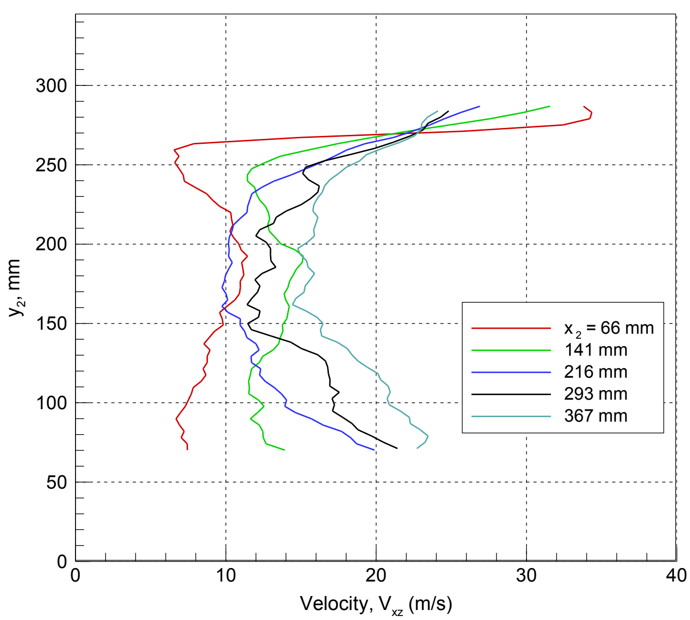

(b) Velocity profiles

Figure 11. Mean velocity field and velocity profiles in the wake (*x-z* plane) of the GMX320 mirror model.

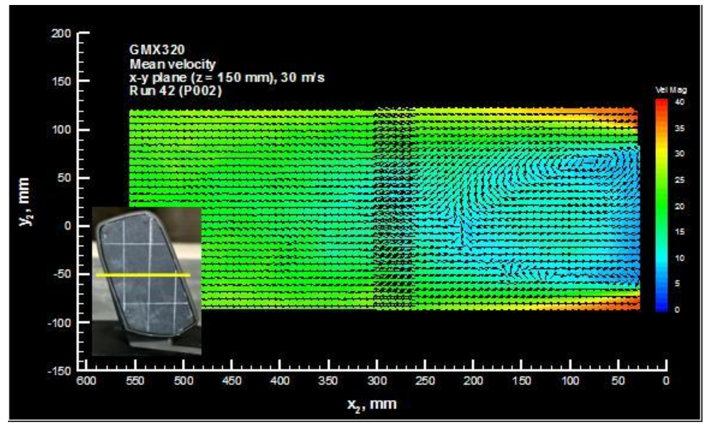

(a) Mean velocity field

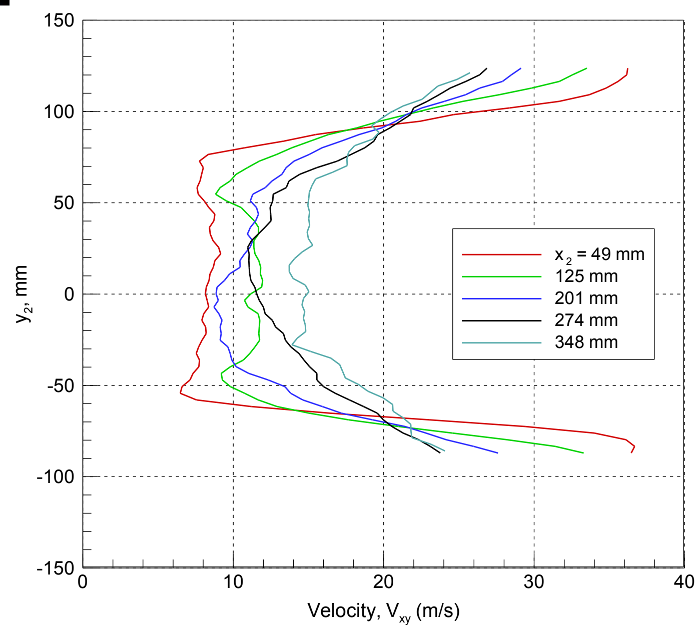

(b) Velocity profiles

Figure 12. Mean velocity field and velocity profiles in the wake (*x-y* plane) of the GMX320 mirror model.

In Figures 11b and 12b, the selection of the velocity profiles taken from the wake of the GMX320 mirror are reasonably consistent, in the respective planes, beyond 125 mm from the reflective surface. When compared to the wake of GMT360, however, the recovery of the velocity deficit in the wake of GMX320 has a spatial lag. This observation can be readily confirmed by a direct comparison of the mean flow fields in the *x-y* plane for the two mirrors, shown in Figures 10a and 12a.

4 Conclusions

Tests in an open-jet wind tunnel were undertaken to examine experimentally the unsteady flow fields behind automobile side-view mirrors. The tests were conducted to characterize the mean and unsteady surface pressures in the wake of two full-scale side-view mirror models, and also to describe the mean velocity field of each wake with PIV measurements. The distinctive geometric of the mirror models may be responsible for significant differences in the makeup of the respective wakes. The results of the mean pressure measurements, for instance, show that the wake of the GMT360 mirror appears to be sensitive to Reynolds number. Meanwhile, unsteady pressure measurements appear to reveal a difference in the character of the trailing vortices in the wake of each mirror. Moreover, PIV measurements depicted wake structures that are as distinctive as the geometry of the mirrors. The experimental data arising from these tests will be used to validate a computational fluid dynamics code that is a component of a larger scheme to predict aero-acoustic noise numerically.

References:

[1] Lee, I. and H.J. Sung, “Multiple-Arrayed Pressure Measurement for Investigation of the Unsteady Flow Structure of a Reattaching Shear Layer”, *Journal of Fluid Mechanics*, Vol. 463, pp. 377-402, 2002.

[2] Melling, A., “Tracer Particles and Seeding for Particle Image Velocimetry”, *Measurment Science and Technology*, Vol. 8, pp. 1406-1416, 1997.

[3] Okuda, Y. and Y. Taniike, “Flow Visualization Around a Three Dimensional Square Prism”, *Journal of Wind Engineering*, No. 37, October 1988. Presented at he International Colloquium on Bluff Body Aerodynamics and Its Applications, Kyoto, Japan, 1988.